Scanning Tunneling Spectroscopic Evidence for Granular Metallic Conductivity in Conducting Polymeric Polyaniline

D. Jeon, J. Kim, M. C. Gallagher, R. F. Willis

Scanning tunneling microscopy (STM) and point-probe electrical conductivity measurements of electrochemically protonated films of the emeraldine-base form of the conducting polymer, polyaniline are reported. The conductivity varies spatially, dependent on the size ($L_M \approx$ 200 to 300 angstroms) of granular metallic regions which relate directly to the inhomogeneous micromorphology of the electrodeposited films. The normalized conductivity at zero bias is observed to increase with doping, indicating an increase in states at the Fermi level. The STM electronic measurements also show regions of negative differential resistance. Negative differential resistance is observed for all samples, although more frequently on less oxidized samples.

Mechanisms of charge conduction in conducting polymers continue to be of increasing interest particularly in regard to the fabrication of metal-insulator-semiconducting devices (*1*) and the nature of the nonlinear electronic response of the self-localized polaron-like charge carriers (*2*). Theoretical studies to date have concentrated on models of single polymer chains doped with random charged defects that produce localized impurity states within a semiconducting band gap (*3*). However, recent experimental work (*4*) has emphasized the importance of understanding the apparent stabilization of the polymeric metallic state against a Peierl's instability (*5*) and the role of interchain coupling (*6*). Theoretically, the electronic "impurity states" of the quasi–one-dimensional polymer become quasi–three-dimensional if the interchain coupling becomes comparable to the scattering rate because of disorder and localization (*7*). This result suggests that the micromorphology of the conducting polymeric system is of importance in the observed insulating-to-metallic transition (*4*).

We report scanning tunneling microscopy (STM) and point-probe electrical measurements of changes in the electrical conductivity with doping of protonated films of the emeraldine-base form of conducting polyaniline (PAN-EB) (*8*). We can use the STM to image the micromorphology and to measure simultaneously changes in the electrical conductivity over the scale of angstroms (*9*). We demonstrate that the statistical variation of many repeated measurements of the conductivity scales directly with the size, $L_M \approx$ 200 to 300 Å, of conducting micromorphological regions. Physically, this result signifies that on the metallic side, the material is inherently inhomogeneous, which lends direct support to the view that conducting PAN is a granular polymeric metal in which the electronic transport occurs by percolation between interconnected conducting grains (*10*). The STM electronic measurements also reveal regions that exhibit negative differential resistance.

The PAN-EB films were prepared by electropolymerization and deposition onto a 2000 Å–thick Au film electrode supported by a silicon wafer substrate. The STM images of the bare Au electrode showed a smooth surface with polycrystalline grain sizes larger than 500 Å. The micromorphology of the electropolymerization from an electrolytic solution (0.5 M H_2SO_4, 0.1 M Na_2SO_4, and 0.1 M aniline monomers) with a constant current density of 70 μA/cm^2 and an electrochemical potential of 0.8 V has been reported (*11*). The conductivity of the films was varied by electrochemical acidification in the same electrolyte after rinsing to remove excess aniline. A distinct electrochromic effect was observed as the films were protonated from the EB form (yellow color) to the emeraldine-salt (ES) form (green) of the conducting polymer (*12*) (Fig. 1A). After drying the films by heating at 50°C in an inert N_2 atmosphere, the film thicknesses used in these experiments were determined to be 500 Å from ellipsometry measurements. This conductive form of PAN is known to remain chemically stable in air, which makes it particularly attractive for device applications compared with other conducting polymers. However, in this work all of the electrical measurements (Fig. 1B) were taken within 1 hour of sample preparation with an STM. The samples were produced at electrochemical potentials of 0.1, 0.2, and 0.5 V. The conductivities vary by a factor of 1000 over this range (*13*), which is similar to that for the doped films reported by Kuzmany *et al.* (*14*) and MacDiamid *et al.* (*15*).

The current-voltage (*I-V*) curves (Fig. 1B) measured with a Pt-Rh tip each represent an average of 25 curves measured at random on the surface and as such are representative of the behavior of each film. The slopes of the *I-V* curves at zero bias voltage, *dI/dV*, increase with increased doping, which means the density of states at the Fermi level of the sample as a whole is increasing, which is consistent with the increasing conductivity of the samples. The fact that *dI/dV* is finite at the Fermi level (zero-bias condition) implies that a finite density of states has developed within the originally insulating (3.6-eV) $\pi - \pi^*$ gap region observed previously (*11*, *12*). This result is consistent with observations of an insulator-metal transition with increasing doping (*16*).

A key experimental result that has shaped recent theoretical interpretations (*17*) of the insulator-metal transition in PAN is the observation that the Pauli susceptibility appears to be proportional to the degree of protonation or oxidation of the polymer (*18*). Physically this result implies that the material is inherently inhomogeneous with regions of protonated metallic "islands" forming a granular structure, which conducts through a thermally activated percolation mechanism (*4*). In order

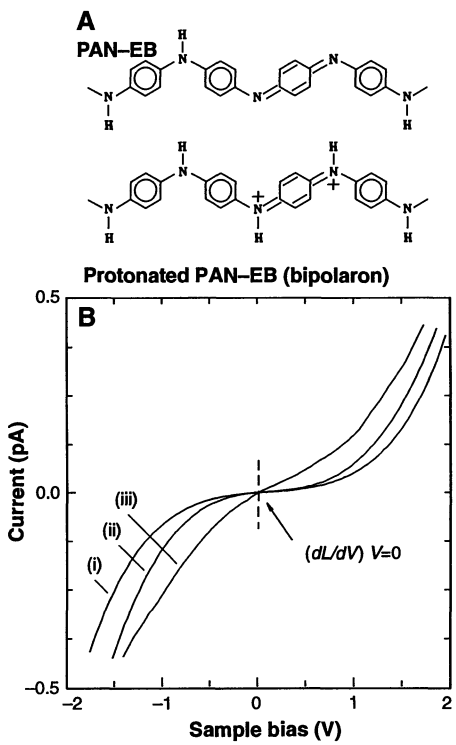

Fig. 1. (**A**) Molecular structure of emeraldine-base form of polyaniline (PAN-EB) and the protonated form showing a bipolaron defect. (**B**) STM current-voltage curves of conducting PAN-EB thin films showing the effect of increasing electrochemical voltage: (i) 0.1; (ii) 0.2; and (iii) 0.5 V. The STM spectra were referenced to 1 nA at a bias of 2.5 V.

Department of Physics, Pennsylvania State University, University Park, PA 16802.

to determine the size of any such "metallic granules" in these particular electropolymerized conducting polymer films, we divided an arbitrary region of the surface into a 5 by 5 square mesh and recorded *I-V* curves similar to those shown in Fig. 1B at each of the 25 crossing points. Each *I-V* curve consisted of 200 data points taken during 1.6 ms, during which time the STM feedback circuitry was momentarily disabled to allow the bias voltage to be linearly swept, ±3 V. In this short time the STM tunneling gap remains constant at the value preset to a reference level of 1 nA of current and a sample bias (9) of 2.5 V. The surface scanning capability of the STM permitted us to vary the mesh size. After recording 25 *I-V* curves from a particular mesh, we determined the ratio of the maximum differential conductivity, $(dI/dV)_M$, at zero bias to its minimum value. A plot of this ratio as a function of the mesh size is shown in Fig. 2. Our argument is that the variation in the measured conductivity at zero bias among each set of 25 *I-V* curves should be almost unity if they correspond to a small area within a single metallic granule (in practice the variation within a single grain would be a value somewhat greater than unity, which would indicate the presence of random fluctuations due to noise). However, as the size is increased, the STM tip would probe the electrical conductivity of different granules within an increasing area such that the variation would increase and eventually flatten out beyond a certain range.

The data (Fig. 2) show this is indeed the case. The average size of a metallic granule is given by the measured value at which the variation begins to increase, $L_M \approx 200$ to 300 Å, which is in surprisingly good agreement with the value (200 to 300 Å) first estimated by Zuo *et al.* (*10*) based on ac conductivity measurements, but a little larger than the "cigar-shaped" metallic regions reported for highly oriented PAN-ES films spin-cast from a solution of *N*-methyl-2-pyrrolidinone (NMP) (~50 Å) (*4*). Recent x-ray experiments by Pouget *et al.* on NMP-cast and HCl-cast samples indicate the presence of crystalline regions of 50 to 100 Å (*19*). These authors conclude that the samples consist of metallic crystallites separated by amorphous regions, which remain unprotonated and form the less conducting barriers. An STM micrograph of the surface of one of our electropolymerized conducting films (Fig. 2A) shows that it is composed of individual polymeric grains of average size in the range given by the variation plot (Fig. 2B). The micromorphology depends on the electrochemical deposition conditions (*11*). Also, the different *I-V* curves in Fig. 1B are not only representative of behavior from films doped to different levels but are seen to a varying degree at different positions on each sample. This result indicates that the doping is nonuniform (*19*) ["textured metallic islands" (*17*)]. A nonuniform dopant distribution was also seen in a previous scanning tunneling spectroscopy study by Bonnell and Angelopoulos (*20*). These workers measured spatial variations in the electronic structure on each film.

In addition to the spatial variations in conductivity, occasionally the *I-V* curves revealed negative differential resistance (NDR) behavior (Fig. 3). Similar behavior has been reported in STM at localized impurity states on Si(111) (*21*). The mechanism of NDR is not entirely clear (*22*), but it does provide direct evidence for charge trapping in localized states. These states decay slowly into the bulk delocalized states, the relaxation time being dependent on inelastic scattering processes (*23*). Although NDR was observed on all films, it was seen more frequently on less oxidized (less conductive) samples. This result is consistent with a heterogeneous dopant distribution, in which the localized states are associated with undoped granules that are more abundant in less conductive films.

When tunneling into granular systems, Coulomb charging energies can become significant. For the 200 Å grains we observe (Fig. 2), the charging energies ($e^2 \cdot 2c$, where e is the electron charge and c is the speed of light) are of the order of 25 meV. At 300 K, this value is too small to give a significant effect. Thermal processes wash out any small discontinuities in the *I-V* spectra that arise from such effects and are not observed.

The electrical properties of electropolymerized thin films of conducting polyaniline can be related to the micromorphology of "textured metallic regions." Regions of NDR are also observed, indicative of charge trapping that is consistent with a nonuniform dopant distribution. The results lend support to the view (*4*, *10*) that the quasi-three-dimensional nature of the electronic states is an important element in determining the electronic behavior of conducting polymer films.

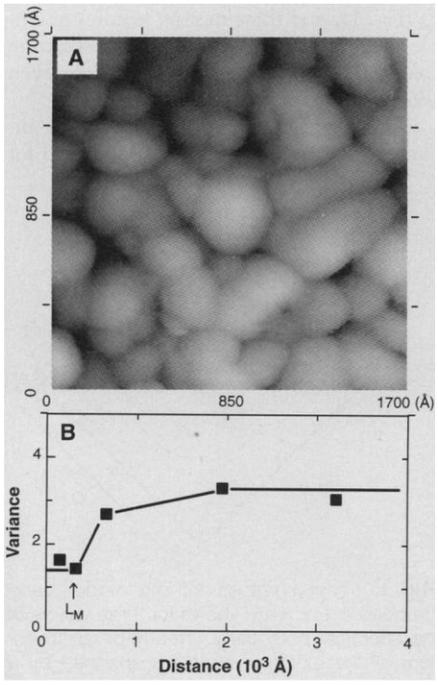

Fig. 2. (**A**) A 1700 Å by 1700 Å gray-scale STM image of the surface micromorphology of the scanned polymer surface, showing average granule sizes L_M of 200 to 300 Å. (**B**) Variance of point-probe electrical conductivity values at zero STM bias voltage $(dI/dV)_M$ as a function of scanned polymer surface area; $L_M \approx 200$ to 300 Å relates to the critical size of metallic regions (high conductivity).

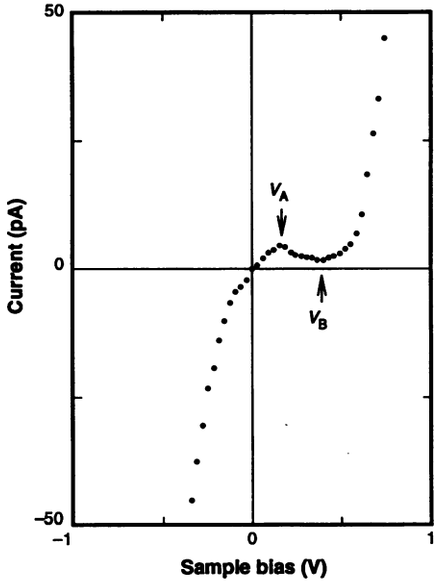

Fig. 3. Negative differential resistance observed for positive sample bias, V_A to V_B, from conducting PAN-EB sample (iii) in Fig. 1.

REFERENCES AND NOTES

1. J. H. Burroughes *et al.*, *Nature* **347**, 539 (1990).
2. A. J. Heeger, S. Kivelson, J. R. Schriefer, W. P. Su, *Rev. Mod. Phys.* **60**, 782 (1988).
3. D. S. Galvao, D. A. dos Santos, B. Laks, C. P. de Melo, M. J. Caldas, *Phys. Rev. Lett.* **63**, 786 (1989); H.-L. Wu and P. Phillips, *ibid.* **66**, 1366 (1991); *Science* **252**, 1805 (1991).
4. Z. H. Wang, C. Li, E. M. Scherr, A. G. MacDiarmid, A. J. Epstein, *Phys. Rev. Lett.* **66**, 1745 (1991).
5. S. A. Kivelson and A. J. Heeger, *ibid.* **55**, 308 (1985); E. M. Conwell, H. A. Mizes, S. Jevadev, *Phys. Rev. B* **40**, 1630 (1989).
6. S. A. Kivelson and A. J. Heeger, *Synth. Met.* **22**, 371 (1988).
7. Y. A. Firsov, in *Localization and Metal Insulator Transition*, H. Fritzsche and D. Adler, Eds. (Plenum, New York, 1985), pp. 471–508.
8. R. deSurville, M. Josefowicz, L. T. Yu, J. Perichon, R. Buvet, *Electrochim. Acta* **13**, 1451 (1968); W. S. Huang, B. D. Humphrey, A. G. MacDiarmid, *J.*

Chem. Soc. Faraday Trans. **82**, 2385 (1986).
9. For a review, see R. J. Hamers, *Annu. Rev. Phys. Chem.* **40**, 531 (1989).
10. F. Zuo, M. Angelopoulos, A. G. MacDiarmid, A. J. Epstein, *Phys. Rev. B* **36**, 3475 (1987); *ibid.* **39**, 3570 (1989).
11. D. Jeon, J. Kim, M. C. Gallagher, R. F. Willis, Y. T. Kim, *J. Vac. Sci. Technol. B* **9**, 1154 (1991).
12. S. Strafström *et al.*, *Phys. Rev. Lett.* **59**, 1464 (1987).
13. E. W. Paul, A. J. Ricco, M. S. Wrighton, *J. Phys. Chem.* **89**, 1441 (1985).
14. H. Kuzmany, N. S. Sariciftci, H. Neugebauer, A. Neckel, *Phys. Rev. Lett.* **60**, 212 (1988).
15. A. G. MacDiarmid, J. C. Chiang, A. F. Richter, A. J. Epstein, *Synth. Met.* **18**, 285 (1987).
16. A. J. Epstein *et al.*, *ibid.*, p. 303.
17. H. H. S. Javadi, K. R. Cromack, M. Angelopoulos, A. G. MacDiarmid, A. J. Epstein, *Phys. Rev. B* **39**, 3579 (1989).
18. J. M. Ginder, A. F. Richter, A. G. MacDiarmid, A. J. Epstein, *Solid State Commun.* **63**, 97 (1987).
19. J. P. Pouget, M. E. Józefowicz, A. J. Epstein, X. Tang, A. G. MacDiarmid, *Macromolecules* **24**, 779 (1991).
20. D. A. Bonnell and M. Angelopoulos, *Synth. Met.* **33**, 301 (1989).
21. R. J. Hamers and R. H. Koch, in *The Physics and Chemistry of SiO_2 and the Si-SiO_2 Interface*, C. Helms and B. Deal, Eds. (Plenum, New York, 1988), p. 201. See also (*11*).
22. For the latest proposal, see R. Garcia, *J. Vac. Sci. Technol. B* **9**, 500 (1991).
23. Also, in the present context, on the height of the barrier and depth of the space-charge region separating the junction from the bulk semiconductor.
24. We thank Y.-T. Kim and K. Vedam for help with preparing the electropolymerized PAN-EB films and R. W. Collins for performing ellipsometry measurements. Supported by NSF grant DMR-8818884 and the Physics Department at Pennsylvania State University (D.J. and J.K.).

10 March 1992; accepted 11 May 1992

Spin Susceptibility Scaling in High-Temperature Superconductors

J. Ruvalds,* C. T. Rieck, J. Zhang, A. Virosztek

The spin response of a nested Fermi surface represented by a tight binding energy band is found to exhibit scaling in frequency divided by temperature within a restricted regime close to half-filling of the band. Computations of the spin susceptibility reveal a surprising momentum variation at various temperatures and frequencies. Neutron scattering data on the high-temperature superconductor $YBa_2Cu_3O_{6+x}$ are analyzed for scaling near a momentum vector that spans nested regions of the orbit. Changes in the Fermi energy remove the scaling properties and reduce the susceptibility to the conventional Fermi liquid behavior of ordinary metals. These results imply that pairing mechanisms of superconductivity need to cope with competing spin density wave and charge density wave instabilities.

The dynamics of electron spins in solids can be described with a susceptibility χ, which in ordinary metals exhibits negligible temperature dependence (*1*). In superconducting copper oxides, however, unusual forms of the spin response are evident in nuclear magnetic resonance (NMR) spectroscopy (*2*) and in neutron scattering studies (*3*). Moreover, small changes in the composition of the cuprates can eliminate the metallic behavior and create an insulating state with antiferromagnetic spin order. It has been proposed that novel spin excitations, including spin polarons (*4*), spin bags (*5*), and spinons (*6*), exist in the cuprates. Hence, understanding spin correlations in the metallic cuprates may provide insight into the mechanism of high-temperature superconductivity.

It is reasonable, therefore, to explore phenomena that could explain the unusual behavior of χ in the cuprates. For example, nesting of Fermi surfaces (*7*), which occurs when sections of an electron orbit in momentum space are nearly parallel, can enhance the electronic susceptibility at a nesting vector $\mathbf{Q}$. This, in turn, may lead to the formation of a spin density wave (SDW) or a charge density wave (CDW) (*8*). A classic example of nesting leads to an SDW in chromium (*9*). These spin and charge instabilities compete with superconductivity, and the corresponding phase diagrams of quasi–one-dimensional systems (*10*) provide relevant examples. In this report, we examine the effects of nesting on spin susceptibility and find an unusual scaling that is in good agreement with recent neutron scattering data.

A representation of nesting by the energy dispersion condition $E(\mathbf{k} + \mathbf{Q}) \cong -E(\mathbf{k})$ provides an analytic solution (*11*) for the lowest order imaginary part of the susceptibility

$$\chi''_0(\mathbf{q},\omega) = -\frac{a^2}{4\pi}\int d^2k \{f[E(\mathbf{k}+\mathbf{q})] - f[E(\mathbf{k})]\}\,\delta[\omega - E(\mathbf{k}+\mathbf{q}) + E(\mathbf{k})] \quad (1)$$

where $f(x) = [\exp(x/T) + 1]^{-1}$ is the Fermi function, and a is the lattice spacing. This ideal approximation allows a straightforward integration over the momentum $\mathbf{k}$ by changing to a variable $x = E(\mathbf{k})$. Thus one obtains

$$\chi''_{NFL}(\mathbf{Q},\omega) \cong \frac{\pi N(0)}{2}\tanh\left(\frac{\omega}{4T}\right) \quad (2)$$

where $N(0)$ is the density of states at the Fermi energy. The variation of this nested Fermi liquid (NFL) response with frequency ω and temperature T is quite different from conventional electron correlations, and the scaling in ω/T is particularly anomalous.

Motivated by the predicted scaling (*11*) and recent neutron scattering probes (*12–18*) of the susceptibility in superconducting crystals of $YBa_2Cu_3O_{6+x}$ and $La_{2-x}Sr_xCuO_4$, we derive limitations on the nesting criteria and find a surprising momentum dependence of the spin correlations on the basis of a tight binding energy band having width $8t$

$$E(\mathbf{k}) = -2t[\cos(ak_x) + \cos(ak_y)] - \mu \quad (3)$$

This model exhibits perfect nesting of a square orbit for a Fermi energy $\mu = 0$ at the nesting vector $\mathbf{Q} = (\pi/a, \pi/a)$. That special case of a half-filled band in two dimensions yields a logarithmic singularity in the density of states and is unstable toward the formation of an SDW for arbitrarily weak Coulomb repulsion. However, lowering μ yields orbits with partial nesting characterized by a wavevector $\mathbf{Q}^* < \mathbf{Q}$ (Fig. 1), and these nesting features resemble the results of sophisticated band structure calculations for the cuprates (*19*, *20*), even though the value of $\mathbf{Q}^*$ may differ.

This model and variations of it that include more terms have been investigated for

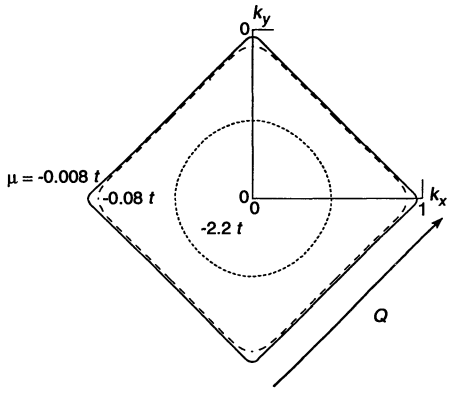

Fig. 1. Fermi surfaces for the model band structure of Eq. 3 are shown for three values of the chemical potential μ. Nearly parallel sections of the electron orbits are spanned by a nesting wave vector $\mathbf{Q}^*$, which is $\mathbf{Q} = (\pi,\pi)/a$ for $\mu = 0$, $\mathbf{Q}^* = 0.999\mathbf{Q}$ for $\mu = -0.008\ t$, and $\mathbf{Q}^* = 0.987\mathbf{Q}$ for $\mu = -0.08\ t$. Scaling of the susceptibility occurs only near half-filling of the band, as in the $\mu = -0.008\ t$ case, and is spoiled by the small curvature of the dashed curve orbit corresponding to $\mu = -0.08\ t$. Conventional Fermi liquid response is found for the nearly spherical orbit shown by the dotted curve with $\mu = -2.2\ t$.

J. Ruvalds, C. T. Rieck, J. Zhang, Physics Department, University of Virginia, Charlottesville, VA 22901.
A. Virosztek, Research Institute for Solid State Physics, 1525 Budapest 114, Post Office Box 49, Hungary.
*New address (effective 15 July 1992): Physics Department, Stanford University, Stanford, CA 94305.